

Nonlinear Observer of Crystal-Size Distribution During Batch Crystallization

T. Bakir, S. Othman, G. Fevotte, and H. Hammouri

LAGEP, UPRES-A CNRS Q 5007/CPE Université Claude Bernard Lyon 1, 43 bd du 11 Nov. 1918, 69622 Villeurbanne Cedex, France

DOI 10.1002/aic.10820

Published online April 6, 2006 in Wiley InterScience (www.interscience.wiley.com).

A high-gain observer was designed to estimate the crystal-size distribution (CSD) in batch crystallization processes. The observer is based on the discretization of population balance equations describing the evolution of the CSD using finite difference method. Due to process impurities and other batch-to-batch variations, the kinetic parameters involved in the dynamic model of the crystallization, relating primary and secondary nucleation in particular, are subject to significant variations. In order to avoid any estimation divergence, an on-line parameter identification algorithm was added to the observer. Assuming that measurements of the nuclei particles are available, the observer is shown to provide a discretized reconstruction of the entire CSD which can be used for control purposes or process supervision. © 2006 American Institute of Chemical Engineers AIChE J, 52: 2188–2197, 2006

Keywords: crystallization processes, high-gain observer, nonlinear identification, population balance equations, crystal-size distribution, finite difference method

Introduction

In batch crystallization as well as in most particulate processes, the CSD (crystal size distribution) influences the quality of the final product. This is particularly important as one considers both application and end-use properties of the crystallized product. However, measuring or estimating the CSD is really difficult and remains an open field of research. Several techniques for the measurement of solute concentration have been used in the past, together with off-line image analysis for the modeling of the time variation of CSD during batch solution crystallizations (for example, by ^{1–6}). However, it is important to notice that no online CSD measurements or estimates were available when such modeling studies were published.

Indeed several sensing *in situ* technologies are actually available which are supposed to yield, at least partially, the CSD during crystallization processes. However, no sensor can really provide accurate measurements of the whole CSD and even the

physical significance of the measured sizes turns out to be questionable. For example, it is well known that the *in situ* focussed beam reflected measurement (FBRM[®]) probe does not yield real particle-size measurements, but chord-length distributions (CLD). In order to address this problem, the aim of this work is to design an on-line observer to reconstruct the entire crystal-size distribution, using both population balance equations and *in situ*, in-line partial measurements. For example, measuring the number of nuclei (that is, the smallest stable crystals) could be performed using the FBRM probe (Lasentec, Metters-Toledo). Worlitschek⁷ has investigated the possibility of restoring CSDs from CLD data using constrained least squares minimization (CLSM). Turbidimetry can also be used to provide quantitative information on the number of small particles in suspension.^{8–10} Such sensors could provide reasonable information for the monitoring of the generation of nuclei even if bigger crystals cannot always satisfactorily be measured (that is, turbidimetry is not suitable for big particles). This is why the reconstruction of the entire CSD from the measurement of the number of nuclei particles would undeniably be a valuable result.

As far as such observer is based on population balance

Correspondence concerning this article should be addressed to T. Bakir at bakir@lagep.univ-lyon1.fr.

equations (PBE) describing the time variations of the CSD, it is essential that the PBE capture the main dynamic features of the process to yield good estimates.

Actually, the crystallization rate (that is, the rate of generation of new crystallized solid) mainly depends on two mechanisms: crystal nucleation and growth. With the assumption of invariant kinetics parameters, the control of such process has been explored¹¹⁻¹³. However, it is clear that the parameters of primary nucleation involved in modeling and control studies may present drifts due to significant irreproducibility during the cooling crystallization process. In other words primary nucleation “seems” to exhibit random features, which can be experimentally observed as batch-to-batch variability. Such variability is inherent to the highly nonlinear features of the crystallization mechanisms, and it is generally attributed to possible impurities in the load of the reactor, and to strong dependency of most basic crystallization phenomena on tiny differences in the operating conditions (for example, presence of small residual crystals on the reactor wall at the beginning of the batch process). Moreover, from a more technical point of view, it is necessary to evaluate the robustness of the estimation process to parameter uncertainties. This is a second reason why the initial values of the nucleation parameters used by the state observer were set to be different from the values which were supposed to relate the “true” experimental nucleation kinetics.

The on-line identification of nucleation parameters was therefore necessary to avoid potential drifts of the observer. In order to deal with this difficulty, the available measurements can also be used to estimate the nucleation parameter(s) in question. In the following, it is shown that combining on-line parameter identification with high-gain CSD estimation allows to efficiently monitor the crystallization process.

The article is organized as follows; first the batch crystallization model is briefly described. The principle of the discretization of the Population Balance Equations (PBE) involved is then exposed. A method for the on-line identification of a “sensitive” primary nucleation parameter is presented, followed by a section devoted to the observer synthesis. The estimation technique is validated through simulation.

Model development

The population balance approach applied to batch crystallizer yields the following partial-differential equation (PDE)

$$\frac{\partial n(x, t)}{\partial t} + G(t) \frac{\partial n(x, t)}{\partial x} = 0 \quad (1)$$

$n(x, t)$ is a number population density function. It represents the number of crystals of size x per unit volume of suspension and per unit of size. In model (Eq. 1), only nucleation and growth will be considered, agglomeration and breakage are not taken into account. The growth kinetic $G(t)$ is assumed to be size independent. The solute concentration balance describing the mass transfer from the liquid to the solid phase is

$$\frac{dV_l(t)C(t)}{dt} + \frac{dV_T(t)C_s(t)}{dt} = 0 \quad (2)$$

$C(t)$ represents the solute concentration, $V_T(t)$ (is the suspension volume, variations of this volume, due to solute mass transfer can be neglected. $C_s(t)$ being the solid concentration, it is easily deduced from the crystal-size distribution (CSD)

$$C_s(t) = \frac{K_v \rho_s}{M_s} \int_{x^*}^{\infty} x^3 n(x, t) dx \quad (3)$$

where K_v is a shape factor (for example, for spherical particles $K_v = \pi/6$), M_s is the molecular weight of the crystallized solid of density ρ_s , and $V_t(t)$ is the solution volume (that is, volume of the continuous phase), which is calculated from the following expression

$$V_t = V_T \left(1 - \frac{M_s}{\rho_s} C_s \right) \quad (4)$$

The crystallizer temperature is given by the energy balance around the cooling jacket wall

$$\sum_{i=1}^3 C p_i n_i \frac{dT_{cr}}{dt} = -\Delta H_c V_T \frac{dC_s}{dt} - U A_c (T_{cr} - T_j) \quad (5)$$

where $C p_i$ and n_i represent, respectively, the molar heat capacities and number of moles of the different components in the crystallizer. T_{cr} and T_j are, respectively, the crystallizer and jacket temperatures. ΔH_c is the crystallization enthalpy. U and A_c are, respectively, the overall heat-transfer coefficient and contact surface of the jacket wall. The solubility, which refers to the solute concentration under saturated conditions, is assumed to obey Van't Hoff equation

$$C_{sat}(T_{cr}) = A e^{-(\Delta H/RT_{cr})} \quad (6)$$

The absolute supersaturation ($C - C_{sat}$) is the driving force of the crystallization process. The overall growth rate, including possible diffusive limitations, is assumed to be represented by the following model. In the literature, values of exponent g are generally assumed to lie between 1 and 2¹⁵

$$G(t) = K_c \frac{M_s}{2\rho_s} \eta (C - C_{sat})^g \quad (7)$$

where K_c represents the kinetic growth rate coefficient, η represents the effectiveness factor, which is the solution of the following equation

$$\left[\frac{K_c}{K_d} (C - C_{sat})^{g-1} \right] \eta + \eta^{(1/g)} + 1 = 0 \quad (8)$$

According to¹⁴, η relates the actual mass flux of solid integrated in the crystal structure to the maximum theoretical flux that would be integrated in the absence of diffusive limitation. For very small particles, η is usually close to 1, which means that the mass-transfer resistance, due to the diffusion of solute

from the bulk to the crystal surface, is negligible for the smaller crystals.

K_d represents the mass-transfer coefficient through diffusion. Analytical solution of Eq. 8 are available if g is equal to one or two, a numerical solution can be considered in the other cases. The nucleation rate B is the result of two competitive nucleation mechanisms. Primary nucleation B_1 takes place in the absence of any crystal in the solution¹⁵

$$B_1 = a_{N1} e^{-(b_{N1}/\ln^2(C/C_{sat}))} \quad (9)$$

where $\beta = C/C_{sat}$ is referred to as the degree of supersaturation.

Secondary nucleation B_2 , which may occur at lower supersaturation level, is favored by the presence of solid in suspension (that is, added in the crystallizer through seeding or generated through primary nucleation)

$$B_2 = a_{N2} M_T^i (C - C_{sat})^j \quad (10)$$

The primary nucleation parameter a_{N1} requires to be identified on-line, a_{N2} and b_{N1} are assumed constant and M_T is the overall mass of solid in suspension. The boundary condition for Eq. 1 is usually set as follows¹⁶

$$n(x^*, t) = \frac{B_N(x^*)}{G(x^*)} = \frac{B}{G} \quad (11)$$

where, according to free energy considerations, only crystal nuclei of critical size x^* are assumed to grow. (that is, for $x < x^*$ the particle will dissolve).

Secondary nucleation clearly appears to be less “explosive” than primary nucleation, and it is known to take place at lower supersaturation values. In other words, the limit curve of metastable zone for secondary nucleation is closer to the solubility curve than the limit curve of metastable zone for primary nucleation.¹⁵ Actually, it is usually assumed that secondary nucleation dominates nucleation phenomena in most industrial crystallization processes. As already mentioned, seeding the crystallizer yields secondary nucleation, provided that the supersaturation level is sufficient. The mass of seed should yet be sufficient to allow significant consumption of solute through crystal growth and, consequently, avoid undesirable primary heterogeneous nucleation burst. Therefore, satisfactory seeding conditions are expected to lead to both moderate increase in the particle number and supersaturation decrease. In the following, unseeded crystallization operations (that is, primary nucleation takes place) are referred to as “case 1” while seeded crystallizations are referred to as “case 2”.

Discretization of the PBE

Many discretization methods were applied to the PBEs (see for example, ¹⁷ and ¹⁸). Finite difference methods which are widely developed in numerical analysis and collocation methods supported by¹⁹ were both applied during this study. The discretization of the crystallization PDE using the first method is rather well developed. Interestingly, finite difference method fits exactly the observer structure. Indeed, the state matrix involved exhibits tridiagonal form. Moreover, the method is

consistent with the physical behavior of the system. Meanwhile, collocation techniques are based on polynomial approximations correlating states from a mathematical point of view, rather than from the physical point of view. The system resulting from the discretization finally turns out to be

$$\begin{cases} \dot{n}_x = \alpha(t) A n_x & \text{with } \alpha(t) = \frac{G(t)}{\Delta x} \\ y = C n_x \end{cases} \quad (12)$$

$$n_x = \begin{bmatrix} n_{x1} \\ n_{x2} \\ n_{x3} \\ \vdots \\ n_{xN-1} \\ n_{xN} \end{bmatrix}, \quad A = \begin{bmatrix} 1 & -1 & 0 & \cdots & 0 \\ \frac{1}{2} & 0 & -\frac{1}{2} & \cdots & 0 \\ 0 & \ddots & \ddots & \ddots & \vdots \\ \vdots & \ddots & 1 & 0 & -\frac{1}{2} \\ 0 & \cdots & 0 & 0 & 0 \end{bmatrix}$$

$$C = [1 \ 0 \ \cdots \ \cdots \ \cdots \ 0].$$

with $n_x \in \Re^N \times \Re^N$ and $C \in \Re^N$. Equations 11 and 12 assume that the number $n_{x1}(t)$ of particles with minimum size that can be measured represents the number of nuclei $n(x^*, t)$. Such assumption is valid if the time required by a given nucleus to grow until the minimum detectable size is supposed to be negligible.

The moment's equations of the CSD are defined by

$$\mu_i = \int_{x^*}^{x^\infty} x^i n(x, t) dx \quad i = 0, 1, 2, 3 \quad (13)$$

The computation of the moments allows evaluating overall parameters characterizing the CSD like the number mean size L_{pop} , and the variation coefficient VC_{pop} which are calculated as follows

$$L_{pop} = \frac{\mu_1}{\mu_0} \quad (14)$$

$$VC_{pop} = \sqrt{\frac{\mu_0 \mu_2}{\mu_1^2} - 1} \quad (15)$$

Identification of primary nucleation parameter a_{N1}

Mechanistic modeling of primary homogeneous nucleation was reported by many authors, and complex models were proposed for both parameters a_{N1} and b_{N1} . However, industrial and laboratory practice clearly show that the reported nucleation models cannot be considered as fully predictive. A good illustration of this problem lies in the fact that, despite reproducible operating conditions, it is very frequent to observe batch-to-batch varying nucleation temperatures related to irreproducible occurrence of the primary nucleation. The resulting variations of nucleation supersaturation, conjugated with the highly nonlinear features of the nucleation kinetics induce dramatic batch-to-batch changes of the particle number. As far as CSD modeling and estimation is concerned, it would, there-

Table 1. Parameters Used for the Simulation of the Crystallization Phenomena, after Marchal²²

Parameter	Definition	Unit	Value
a_{N1}	Pre-exponential primary homogeneous nucleation parameter	$\text{nb} \cdot \text{m}^{-3} \cdot \text{s}^{-1}$	Computed from 15, 24
b_{N1}	Exponential primary homogeneous nucleation parameter	No dimension	0.69
a_{N2}	Secondary nucleation parameter	$\text{nb} \cdot \text{m}^{3(i+j-1)} \cdot \text{mol}^{-i-j} \cdot \text{s}^{-1}$	1440
K_c	Growth constant	$\text{mol}^{(1-g)} \cdot \text{m}^{(3g-2)} \cdot \text{s}^{-1}$	$1.57 \cdot 10^{-2}$
i	Exponent	No dimension	1.968
j	Exponent	No dimension	1
g	Exponent	No dimension	2
M_s	Molar mass of the solute	$\text{Kg} \cdot \text{mol}^{-1}$	$146.14 \cdot 10^{-3}$
ρ_s	Density of the solute	$\text{Kg} \cdot \text{m}^{-3}$	1360
K_v	Crystal shape factor	No dimension	$\pi/6$
Cp_1	Solute molar heat capacity	$\text{J} \cdot \text{K}^{-1} \cdot \text{mol}^{-1}$	3.72
Cp_2	Molar heat capacity of the solid	$\text{J} \cdot \text{K}^{-1} \cdot \text{mol}^{-1}$	7.44
Cp_3	Molar heat capacity of water	$\text{J} \cdot \text{K}^{-1} \cdot \text{mol}^{-1}$	75.33
ΔH_c	Crystallization enthalpy	$\text{J} \cdot \text{mol}^{-1}$	-48000
U	Overall heat-transfer coefficient through the jacket	$\text{W} \cdot \text{m}^{-2} \cdot \text{K}^{-1}$	1000
A_c	Contact surface of the jacket	m^2	$2.2 \cdot 10^{-2}$

fore, be illusory to rely on constant nucleation parameter values. In the following approach, it is assumed that a_{N1} is a highly uncertain parameter, while b_{N1} is assumed constant, with possible differences with respect to the simulated “true” value. In order to estimate the time variations of the CSD, a state observer was designed assuming that measurements of the number of the initial particles (that is, the nuclei) are performed. In order to strengthen the estimation scheme, parameter a_{N1} was also estimated. A Levenberg-Marquardt algorithm was used to perform such identification, it is based on the minimization of the following quadratic error criterion

$$J(\theta) = \sum_{i=1}^N (y_m(t_i) - y(t_i, \theta))^2 = \sum_{i=1}^N (e_i(\theta))^2 \quad (16)$$

The identification is performed on adequate sliding horizon of points. Measurement and pseudomeasurements being available, the estimation of the crystal-size distributions, and the calculation of the moments resulting from this estimation can be performed. It is worth noting that, in contradiction with CSD measurements, solute concentration measurements are currently available in-line.^{20,21} For example ATR FTIR *in situ* solute concentration measurements were successfully performed for several model crystallization systems. Using such technique, our group has reported relative uncertainties of the order of 1–2%, in the case of various organic batch crystallization operations (see, for example, ^{20,26,27}). These latter measurements can be used to compute the time variations of supersaturation and, therefore, the nucleation and growth kinetics leading to the number of generated nuclei, according to Eq. 11. The estimated values of are then considered as pseudomeasurements which can be updated using any infrequent and/or off-line CSD measurement, allowing variations of parameter a_{N1} to be identified. Such identification of the nucleation kinetic rate B_j improves the observer convergence.

It is clear that, given the structure of the primary nucleation model, the identification of both parameters a_{N1} and b_{N1} is impossible from the measurements which are assumed to be available. However, preliminary simulations have clearly shown that for any reasonably uncertain initial value of, the observer yields appropriate value of such that the reconstructed CSD is satisfactory. For example, in the following b_{N1} was

assumed to be equal to 0.69 (see Table 1), which led to the time variations of displayed in Figure 2. Setting b_{N1} to 0.9 obviously yielded different variations of parameter a_{N1} , with a maximum of $0.6 \cdot 10^{12} \text{ nb} \cdot \text{m}^{-3} \cdot \text{s}^{-1}$. However, in both cases, the two estimated pairs (a_{N1} and b_{N1}) produced really similar CSD profiles.

High gain observer synthesis

In the case of single output systems, the high gain observer is dedicated to the uniformly observable systems class of the following form

$$\begin{cases} \dot{z} = f(z) + \sum_{i=1}^P u_i g_i(z) \\ y = h(x) \end{cases} \quad (17)$$

where

$$z \in \mathbb{R}^N, \quad y \in \mathbb{R}, \quad u \in \mathbb{R}^P$$

System (Eq. 17) is said to be uniformly observable if for any two initial states $z \neq \bar{z}$ and every admissible inputs defined on any $[0, T]$, there exists $t \in [0, T]$ such that $y(z, u, t) \neq y(\bar{z}, u, t)$, where $y(z, u, t)$ is the output associated to the initial state z and the input u . This means that the observability of the system is not affected by the variation of the input u in the interval of observation $[0, T]$.

Here, system (Eq. 17) takes the particular form of system (Eq. 12), which is clearly observable due to its triangular form. Indeed, in this particular case, the structure of the different differential equations (matrix A) shows that, on the observation interval, a given output trajectory implies a unique solution of the set of the other crystal classes. Such observability can be proved using the well known Kalman criterion: $\text{rank} [(C, CA, \dots, CA^{N-1})] = N$.

The canonical form may be used to construct an exponential observer for system (Eq. 12) under the following technical assumption $\exists \gamma, \xi$ with $0 < \gamma \leq \xi, \forall t \leq 0 : \gamma \leq \alpha(t) \leq \xi$ for some constant γ and ξ .

As $\alpha(t)$ represents the growth kinetic which is positive and

bounded, this assumption is not restrictive in the case of crystallization processes.

In the case of continuous measurements, a candidate exponential observer for the system is given by ²² and ²³

$$\dot{\hat{z}}(t) = \alpha(t)A\hat{z}(t) - \alpha(t)S_{\theta}^{-1}C^T(C\hat{z}(t) - y(t)) \quad (18)$$

where S is symmetric positive definite matrix given by the following equation

$$\dot{S}_{\theta}(t) = -\theta S_{\theta}(t) - A^T S_{\theta}(t) - S_{\theta}(t)A + C^T C \quad (19)$$

If $\alpha(t)$ is negative for any time $t > 0$, the sign of the correction term should be changed

$$\dot{\hat{z}}(t) = \alpha(t)A\hat{z}(t) + \alpha(t)S_{\theta}^{-1}C^T(C\hat{z}(t) - y(t)) \quad (20)$$

Case 2 requires to apply the previous model when seeding is performed. Here the discretization is based on about 50 samples. This number was chosen to allow satisfactory accuracy of the model representation. The same number of samples was used in the observer synthesis, while in case 1, N was set to 100 so as to improve the model accuracy. Such a number is not harmful to the observer computation time, and could be reduced to a quarter $N_{observer} = 25$. The latter simplification allows one to significantly reduce the observer variables, and consequently, allows saving significant computation time. The model-predicted variables, and the corresponding estimates will be compared in the next section.

For case 1 (unseeded solution), matrix A in Eq. 12 is replaced by

$$A = \begin{bmatrix} \frac{1}{ratio} & \frac{-1}{ratio} & 0 & \cdots & 0 \\ \frac{1}{2ratio} & 0 & \frac{-1}{2ratio} & \cdots & 0 \\ 0 & \ddots & \ddots & \ddots & \vdots \\ \vdots & \ddots & \frac{1}{2ratio} & 0 & \frac{-1}{2ratio} \\ 0 & \cdots & 0 & 0 & 0 \end{bmatrix}$$

with

$$ratio = \frac{N}{N_{observer}}$$

In other words

$$A_1 = \frac{A}{ratio}$$

In order to make use of the previous observer structure, we consider the following change of variables

$$\alpha_1(t) = \frac{\alpha(t)}{ratio} = \frac{G(t)}{\Delta x ratio} \quad (21)$$

The new system is given by

$$\begin{cases} \dot{n}_{x_{observer}}(t) = \alpha_1(t)A n_{x_{observer}}(t) \\ y(t) = C n_{x_{observer}}(t) \end{cases} \quad (22)$$

Despite the change of coordinates the structure remains unchanged. Reducing the number of variable in the gain matrix S allows saving integration computation time. The new number of S components being $(1 + N_1)(N_1 - 1)/2$.

Another alternative is to use the following diffeomorphism

$$\begin{aligned} \phi: \mathbb{R}^N &\rightarrow \mathbb{R}^N \\ z &\rightarrow [h, L_f(h), \dots, L_f^{N-1}(h)] \end{aligned}$$

Such diffeomorphism transforms system (Eq. 12) into the observable canonical form with

$$A_2 = \begin{bmatrix} 0 & 1 & \cdots & 0 \\ 0 & 0 & \ddots & \vdots \\ \vdots & \vdots & \ddots & 1 \\ 0 & 0 & \cdots & 0 \end{bmatrix}, \quad C_2 = [1 \ 0 \ \cdots \ 0]$$

The resulting observer exhibits the following form:

$$\dot{\hat{z}} = \alpha(t)A_z - \alpha(t)\left(\frac{\partial \phi}{\partial z}(\hat{z}, t)\right)^{-1} S_{\theta}^{-1}C_2^T(C_2\hat{z} - y) \quad (23)$$

where S_{θ} is given by the Lyapunov equation

$$\theta S_{\theta} + A_2^T S_{\theta} + S_{\theta} A_2 = C_2^T C_2 \quad (24)$$

The terms of matrix $S_{\theta} = [S_{\theta}(l, k)]_{1 \leq l, k \leq N}$ are given by

$$S_{\theta}(l, k) = \frac{(-1)^{l+k} D_{l+k-2}^{k-1}}{\theta^{l+k-1}} \quad (25)$$

with

$$D_n^k = \frac{n!}{(n-k)!k!} \quad (26)$$

In this case, the calculation of ϕ is straightforward because matrix A is constant. The result is given by the following equation

$$\phi = \phi_1 z \quad (27)$$

with

$$\phi_1 = [C, CA, \dots, CA^{N-1}] \quad (28)$$

thus

$$\left(\frac{\partial \phi}{\partial z}(\hat{z}, t)\right)^{-1} = [C, CA, \dots, CA^{N-1}] \quad (29)$$

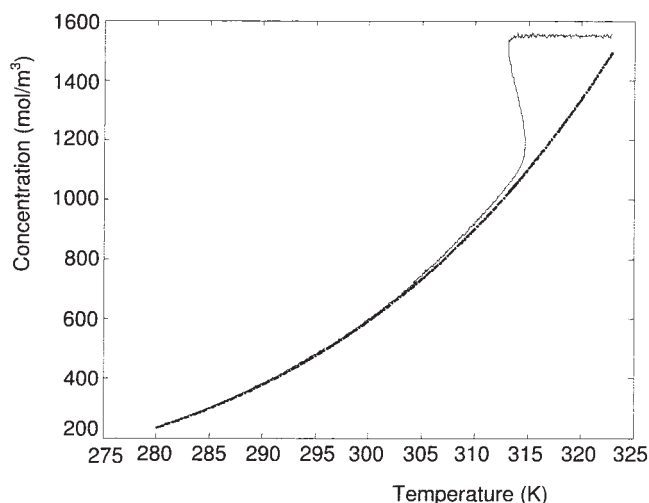


Figure 1. Solubility curve (dashed line) and simulation of the concentration profile (solid line) during unseeded batch cooling crystallization of adipic acid.

Simulation Results and Discussion

Simulation conditions

The parameters used to simulate an industrial batch crystallization process were taken from the in depth investigation of the crystallization of adipic acid in water reported by Marchal²⁴. Primary homogeneous nucleation models were also taken from²⁵. The cooling fluid in the jacket was assumed to be brine at 0°C. Table 1 summarizes both the kinetic and operating parameter values which were used during the simulation.

Simulation results and discussion; case 1

Figure 1 displays the concentration diagram of a typical simulated unseeded batch crystallization process. The model simulated operating conditions are the following

- The initial undersaturated adipic acid solution is kept to 50 °C (323 K). The initial solute concentration is 1550 mol/m³, while the corresponding solubility is about 1500 mol/m³.
- Cooling is assumed through temperature controlled brine initially kept at 320 K (that is, the initial temperature difference between the jacket and the solution is 3°C). The set point trajectory for the cooling brine tracks a constant rate of -1 °C/min until the final crystallizer temperature is reached (280 K).

Stirring effects are not explicitly taken into account in the crystallization model, even though it is well-known that nucleation phenomena are likely to strongly depend on the stirring power. However, it is assumed that such effects are indirectly represented through possible variations of the nucleation kinetic parameters.

The width of metastable zone appears to be rather large while the residual supersaturation following the initial nucleation and growth process remains very low. Indeed, Figure 1 shows that due to primary nucleation and growth of the newly generated particles, the solute concentration starts to decrease at about 313 K. the corresponding solubility is about 1,020 mol/m³, and the initial supersaturation is, therefore, $C - C_{sat} =$

1,550–1,020 = 530 mol/m³. This latter point, together with the fast return to solubility after primary nucleation indicates that the simulated growth rate is sufficient to allow fast consumption of the solute during the cooling process after nucleation. This experimental behavior is indeed observed during the industrial crystallization of adipic acid in water. Consequently, due to the low supersaturation values, reduced secondary nucleation is expected during the continuation of the batch process.

Identification of parameter is shown in Figure 2. Despite the simulation of a significant initial uncertainty, the convergence appears to be very fast at the onset of primary nucleation (that is, after about 140 s, which corresponds to $T = 312$ K the nucleation process is observed). The identification then appears to be really stable, accurate and efficient in tracking slight temperature variations of parameter a_{N1} . However, after about 400 s, the estimation process loses its efficiency, which is neither surprising nor detrimental since, due to negligible supersaturation level, the nucleation process is almost terminated.

Figure 3 displays the time variations of the number of nuclei which are assumed to be imperfectly measured. A noise (gaussian noise with variance of about 0,38) was added to the “real” simulated data of the number of generated nuclei (that is, as outlined earlier, crystals contained in the smallest size class.) Again, the convergence of the estimated number of small particles appears to be satisfactory.

As examples of the estimation of particle numbers in the different size classes, Figures 4 and 5 show a comparison between the evolutions of the numbers of particles in the 9th and 57th model classes, respectively. These two classes of size correspond to 18 μm and 104 μm, respectively. The classes in Figures 4 and 5 were arbitrarily selected to illustrate the convergence and the performance of the observer. The whole range of other simulated classes yielded similar results. In Figure 4, the estimation of the number of small particles

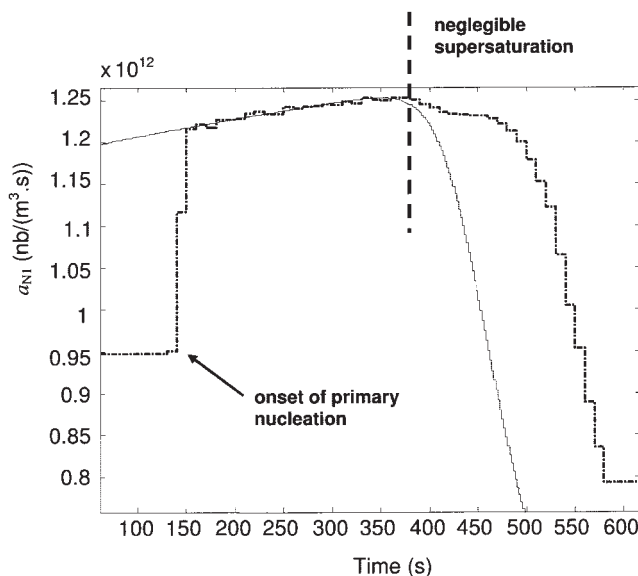


Figure 2. Simulated variations of the primary nucleation parameter a_{N1} (continuous line) and estimates using Levenberg-Marquardt Algorithm (dashed line)

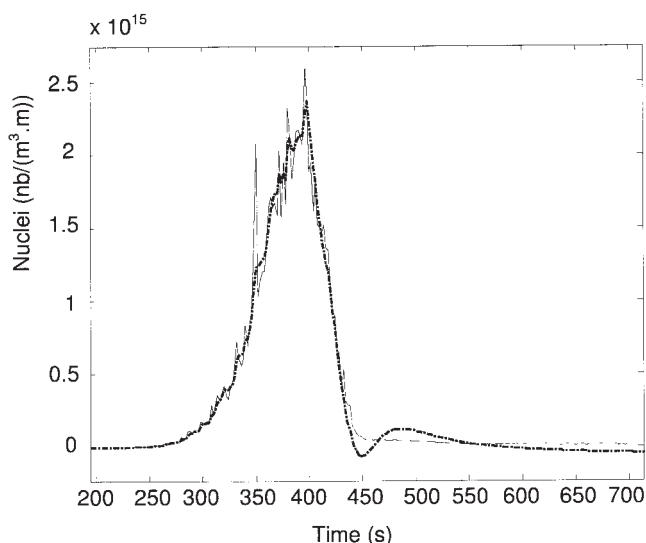


Figure 3. Simulated measurement of the number of nuclei (continuous line) and estimates (dashed line) during unseeded batch cooling crystallization.

appears to be less stable than for bigger crystals in Figure 5. This is simply due to the fact that big particles do not disappear through growth at the end of the batch process while, due to the cancellation of primary nucleation when supersaturation tends toward zero, the growth of smaller particles make them vanish in the size distribution.

Even though they provide reduced information about the CSD, the moments of the size distribution can be considered as representative of the accuracy of the reconstruction of the whole size distribution. From this point of view, Figure 6 represents the third moment which is required to compute the

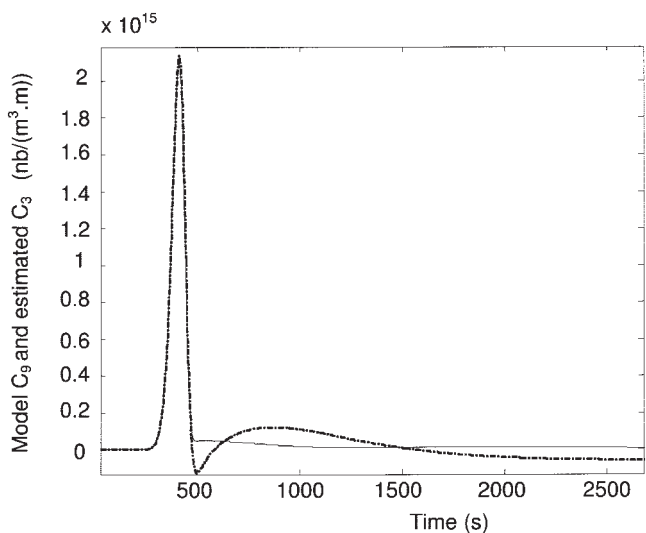


Figure 4. Simulation (solid line) and reconstructed time variations (dashed line) of the 9th size class (18 μm) of the model (that is, the 3rd size class of the state observer) during unseeded batch cooling crystallization.

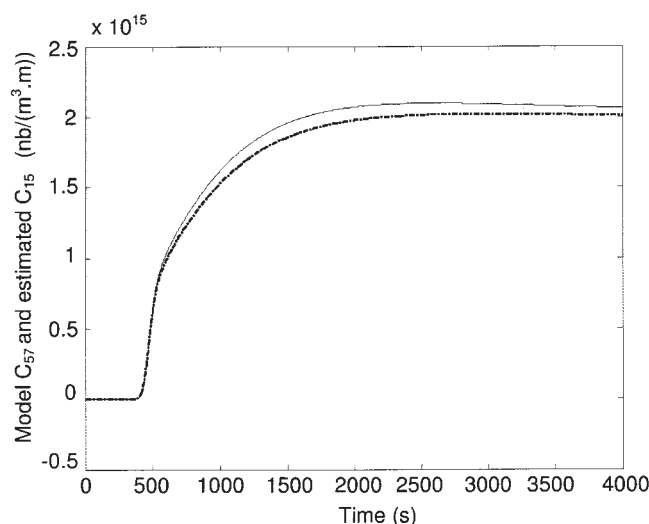


Figure 5. Simulation (solid line) and reconstructed time variations (dashed line) of the 57th size class (104 μm) of the model (that is, the 15th size class of the state observer) during unseeded batch cooling crystallization.

weight average particle size. Figure 7 displays the number average crystal size (that is, the ratio $L_{\text{mean}} = (\mu_1/\mu_0)$). It appears that, except before the occurrence of significant primary nucleation (that is, before the time when it is meaningless to estimate the particle sizes), the average size and the moments are well estimated by the high-gain observer. Finally, a presentation of the simulated CSD, compared with the reconstructed CSD obtained with reduced number of size classes, is given in Figures 8 and 9. As expected from the previous comparisons, the fit between the two plots is satisfactory.

Simulation results and discussion, case 2

Seeded crystallizations (that is, case 2) are usually performed in order to circumvent the effects of the primary ho-

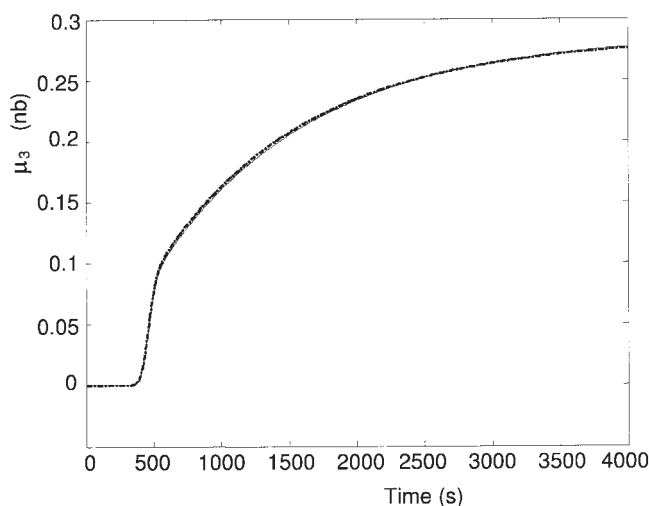


Figure 6. Simulation (solid line) and reconstructed time variations (dashed line) of the third moment of the size distribution during unseeded batch cooling crystallization.

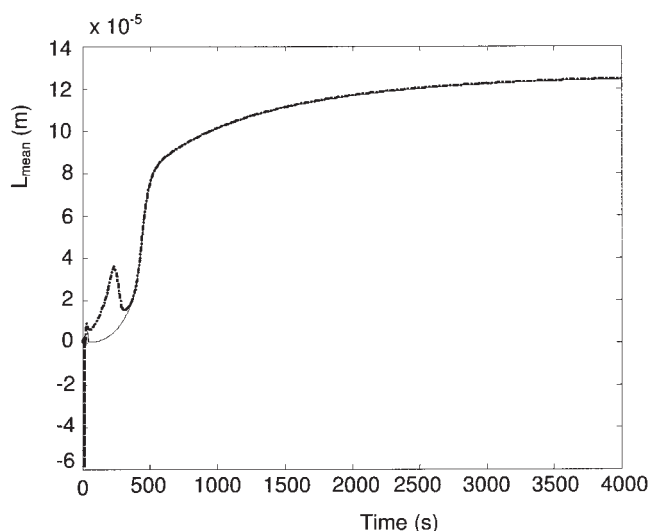


Figure 7. Simulation (solid line) and reconstructed time variations (dashed line) of the number average particle size during unseeded batch cooling crystallization.

mogeneous nucleation burst, and, therefore, reduce the detrimental effect of too large a number of initial particles on the final CSD. Simulating such operating mode requires the knowledge of both the number and size distribution of the seed particles. In the following, the mass of seed is set to 5% of the overall expected mass of crystallized product, and its average particle size is of the order of $20\ \mu\text{m}$. In order to evaluate the convergence of the observer, a 10% uncertainty was added to every class of the initial seed CSD (that is, to the simulated “real” seed CSD) and introduced as initial CSD estimate. Figure 10 shows the difference between the “actual” seed CSD, and the initial guess used by the observer.

Seeding batch crystallizers results in lower initial supersaturation levels, due to the growth of seeds. Consequently, the variation of the CSD during seeded crystallizations (case 2) is slower than during unseeded operations. This is the reason why

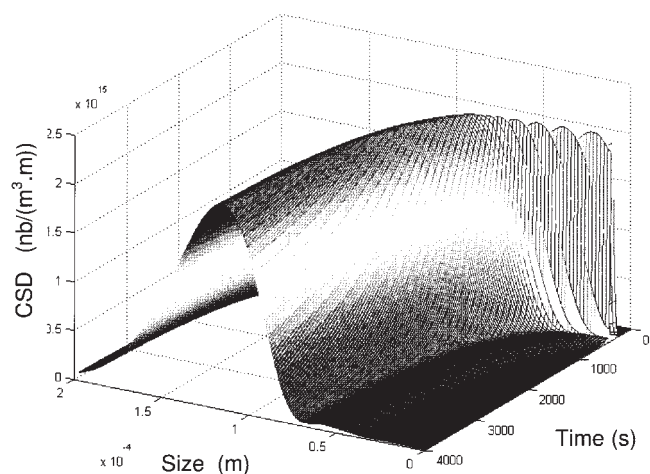


Figure 8. Simulation of the time variations of the CSD during unseeded batch cooling crystallization of adipic acid.

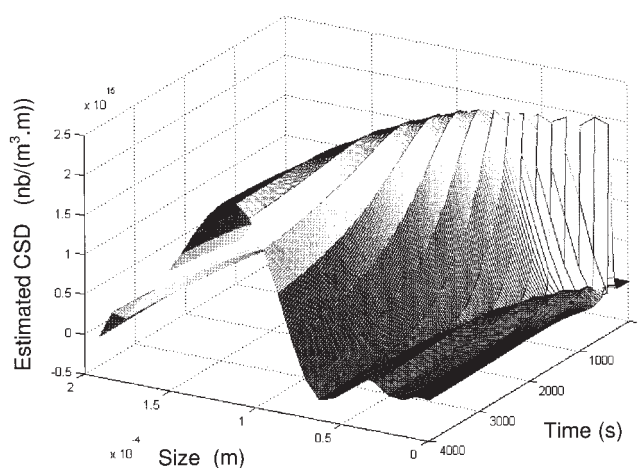


Figure 9. Estimation of the time variations of the CSD during unseeded batch cooling crystallization of adipic acid.

satisfactory operation of the state observer during seeded operations was found to require fewer measurements than during “case 1” situations. Figure 11 demonstrates the very fast convergence of the estimation algorithm to reconstruct the time variations of the number of nuclei particles during the seeded process.

Finally, Figure 12 shows a rather satisfactory comparison between both estimated and simulated number average particle sizes L_{mean} . At the beginning of the crystallization, as expected, the average size is overestimated, due to the initial underestimation of the particle number (that is, less particles from bigger size classes). At the end of the batch process, the relative uncertainty of the estimates is of the order of 5%.

Conclusions

Actually, the more sophisticated commercially available particle analyzers are unable to provide accurate and reliable

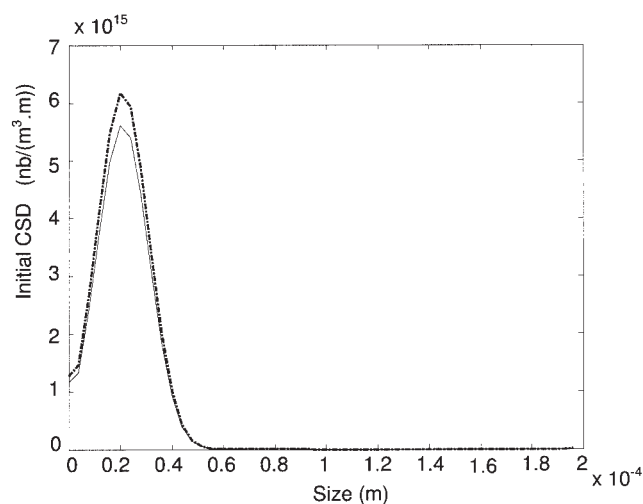


Figure 10. (Dashed line) Initial observer CSD (A 10% uncertainty was added to the simulated seed CSD), and (solid line) simulated seed CSD during “case 2” batch cooling crystallization.

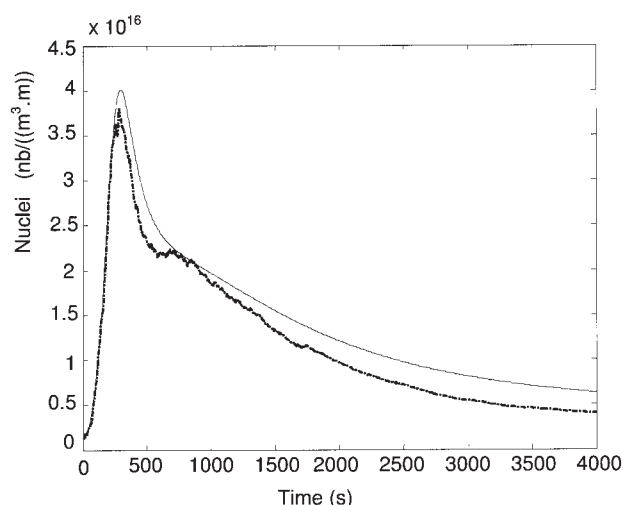


Figure 11. Simulated measurement of the number of nuclei (continuous line) and estimates (dashed line) during seeded batch cooling crystallization.

measurements of the “real” particle-size distribution during crystallization processes. For both theoretical and numerical reasons, even for suspensions exhibiting ideal properties (such as, spherical particle shapes and monomodal distributions) extracting indicative CSD from sensors raw data remains an open problem. In order to address this important difficulty, one can expect powerful state estimation techniques to allow the reconstruction of CSD from partial measurements of the size distribution.

An observation approach based on the design of a high-gain observer is presented here, which is shown to be efficient in simulation. The proposed state observer assumes in-line measurements of the number of nuclei particles (that is, of the smallest stable crystals in suspension). Such requirement,

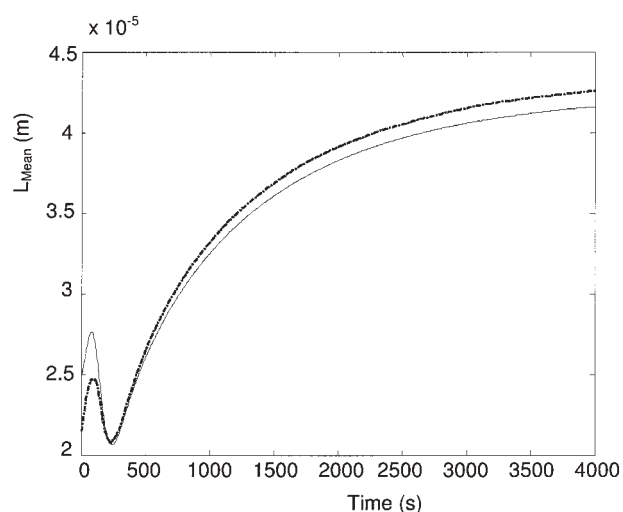


Figure 12. Simulation (solid line) and reconstructed time variations (dashed line) of the number average particle size during seeded batch cooling crystallization.

which indeed is rather demanding, is not that unrealistic due to the significant progresses accomplished in the field of particle sensing technologies together with the possibility of using physical or statistical models to extract dependable nucleation data from imperfect measurements. The infinite dimensional system describing the time variations of the particle sizes was discretized, allowing a state formulation of the population balance equations. Even though it is theoretically possible, the estimation of huge a number of variables (the size classes) is numerically difficult to implement. This is why a reduction of the order of the state observer was performed. Primary nucleation was assumed to be the main crystallization mechanism governing the CSD and particular attention was paid to the potential batch-to-batch variations of the pre-exponential parameter involved in the primary nucleation rate model. In order to increase the robustness of the observer, the batch-to-batch and time variations of were identified using a Levenberg-Marquardt algorithm. Through simulation studies, it is shown that the whole state observation strategy is really efficient in reconstructing the time evolutions of the CSD, as far as significant variations of the particle size take place (that is, when unegligible supersaturation is generated as the driving force of crystal growth).

Literature Cited

1. Braatz RD, Hasebe S. Particle size and shape control in crystallization processes. *AIChE Symp Series*. 2002;326:307-327.
2. Feng L, Berglund KA. “ATR-FTIR” for determining optimal cooling curves for batch crystallization of succinic acid. *Crystal Growth and Design*. 2002;5:449-452. [3] Puel F, Févotte G, Klein JP. Simulation and analysis of industrial crystallization processes through multidimensional population balance equations. Part 1: a resolution algorithm based on the method of classes. *Chem Eng Sci*. 2003;58:3715-3727.
4. Rawlings JP, Miller SM, Witkowski WR. Model identification and control of solution crystallization process : a review. *Ind Eng Chem Res*. 1993;32:1275-1296.
5. Rohani S. Crystallization kinetics, modeling and control: a review. *Trends in Chem Eng*. 1998;5:173-193.
6. Worlitschek J, Mazzotti M. Model-based optimization of particle size distribution in batch-cooling crystallization of paracetamol. *Crystal Growth and Design*. 2004;4:891-903.
7. Worlitschek J. *Monitoring, modeling and optimization of batch cooling crystallization.*, ETH n° 15189. Zurich: Germany; 2003. PhD diss.
8. Zollars, Richard L. Turbidimetric method for on-line determination of latex particle number and particle size distribution. *J of Colloid and Interface Sci*. 1980; 74(1), 163-72.
9. Herri JM, Gruy F, Pic JS, Counil M, Cingotti B, Sinquin A. Interest of *in situ* turbidimetry for the characterization of methane hydrate crystallization: application to the study of kinetic inhibitors. *Chem Eng Sci*. 1999;54(12):1849-1858.
10. Moscosa-Santillan M, Bals O, Fauduet H, Porte C, Delacroix A. Study of batch crystallization and determination of an alternative temperature-time profile by on-line turbidity analysis - application to glycine crystallization. *Chem Eng Sci*. 2000;55(18):3759-3770.
11. Jones AG. Optimal operation of a batch cooling crystallizer. *Chem Eng Sci*. 1974;29:1075-1087.
12. Rohani S. Self-tuning control of crystal size distribution in a cooling batch crystallizer. *Chem Eng Sci*. 1990;45:3457-3466.
13. Zoltan KN, Richard DB. Open loop and closed-loop robust optimal control of batch processes using distributional and worst case analysis. *J of Proc Contr*. 2004;411-422.
14. Garside J. The concept of effectiveness factors in crystal growth. *Chem Eng Sci*. 1971;26:1425-1431.
15. Mersmann A. *Crystallization Technology Handbook*. 2nd ed. Mersmann. New York: Marcel Dekker; 2002.
16. Ramkrishna, D.. *Population balances. Theory and applications to particulate systems in engineering*. New York: Academic Press; 2000.
17. Kumar, S., Ramkrishna D. On the solution of population balance

- equations by discretization-III. Nucleation, growth and aggregation of particles. *Chem Eng Sci.* 1997;52:4659-4679.
18. Liu Y, Cameron IT. A new wavelet-based adaptive method for solving population balance equations. *Powder Technology.* 2003;181-188.
 19. Villadsen JV, Stewart WE. Solution of boundary-value problems by orthogonal collocation. *Chem Eng Sci.* 1966;22:1483-1501.
 20. Fevotte G. New perspectives for the on-line monitoring of pharmaceutical crystallization processes using in situ infrared spectroscopy. *Intl J of Pharmaceutics.* 2002;241(2):263-278.
 21. Yu L. X., Lionberger R. A., Raw A. S., D'Costa R., Wu H., Hussain A. S. "Applications of process analytical technology to crystallization processes." *Advanced Drug Delivery Reviews.* 2004;56(3): 349-369.
 22. Farza M, Hammouri H, Othman S, Busawon K. Nonlinear observer for parameter estimation in bioprocesses. *Chem Eng Sci.* 1997;52:4251-4267.
 23. Gauthier JP, Hammouri H, Othman S. A simple observer for non linear systems Application to bioreactors. *IEEE Trans Automat Control.* 1992;37:875-880.
 24. Marchal PG. *énié de la cristallisation: application à l'acide adipique.* Thèse, Institut National Polytechnique de Lorraine. Nancy: France; 1989.
 25. Mersmann A, Braun B, Löfflmann M. Prediction of crystallization coefficients of the population balance. *Chem Eng Sci.* 2000;57:4267-4275.
 26. Lewiner F, Klein JP, Puel F, Fevotte G. On-line ATR FTIR measurement of supersaturation during solution crystallization processes. Calibration and applications on three solute/solvent systems. *Chem Eng Sci.* 2001;56(6):2069-2084.
 27. Oullion MP, Fevotte G, Klein JP, Righini S, Carvin P. Monitoring and modeling batch crystallization of a food ingredient. 16th *International Symposium of Industrial Crystallization ISIC'16.* Dresde. Sept. 11-14; 2005.

Manuscript received May 19, 2005, and revision received Jan 25, 2006.